

Explicit Simulation of Midlatitude Cumulus Ensembles: Comparison with ARM Data

KUAN-MAN XU AND DAVID A. RANDALL

Department of Atmospheric Science, Colorado State University, Fort Collins, Colorado

(Manuscript received 12 August 1998, in final form 17 November 1999)

ABSTRACT

This study describes some results from several simulations of cumulus ensembles at the Southern Great Plains site of the Atmospheric Radiation Measurement (ARM) program during the July 1995 Intensive Observation Period (IOP). A 2D cloud ensemble model (CEM) is used to simulate the macroscopic properties of midlatitude cumulus ensembles. The observed large-scale, horizontal advective tendencies and large-scale vertical velocity or the total advective tendencies are used to drive the CEM, in addition to nudging of the simulated, domain-averaged horizontal wind components toward the observed winds.

A detailed comparison with available observations and tropical convection is made in this study. In general, the CEM-simulated results agree reasonably well with the available observations from the July 1995 IOP. The differences between simulations and observations are, however, much larger than those obtained in tropical cases, especially those based on the Global Atmospheric Research Program Atlantic Tropical Experiment Phase III data. Significant differences exist between the statistical properties of tropical and midlatitude cumulus convection, especially in the vertical structures of the cumulus mass fluxes, apparent heat source (Q_1), and apparent moisture sink (Q_2). The strong variations of the subcloud-layer thermodynamic structure and the surface fluxes in midlatitude continents have large impacts on the heat and moisture budgets. The radiative budgets and satellite-observed cloud amounts are also compared with observations. Although the agreements are reasonably good, some deficiencies of the simulations and inadequate accuracy of large-scale advective tendencies can be clearly seen from the comparisons. Sensitivity tests are performed to address these issues.

1. Introduction

This study is a part of the Atmospheric Radiation Measurement (ARM; Stokes and Schwartz 1994) program's single-column model (SCM) intercomparison study (Ghan et al. 2000), which compares the performance of various SCMs and a two-dimensional (2D) cloud ensemble model (CEM) with ARM Intensive Observation Period (IOP) datasets by providing a common set of forcing data and supporting data for running the SCMs and CEMs. The goal of the intercomparison study is to identify the data requirements for the ARM SCM research and to facilitate scientific advances by promoting collaborations among ARM Science Team members through common activities; specifically, to improve the representations of cloud formative/dissipative processes in general circulation models (GCMs) and their interactions with radiation. This is one of the two overall objectives of the ARM program (Stokes and Schwartz 1994). The use of SCMs and CEMs for achieving such a goal was reviewed by Randall et al. (1996).

A CEM resolves individual clouds and their meso-

scale organization but covers a large horizontal domain. It allows several clouds of various sizes to develop simultaneously and randomly inside the model domain. Thus, the major difference between an SCM and a CEM is that cloud-scale circulations are explicitly resolved in a CEM, but must be parameterized in an SCM. CEMs can simulate bulk cloud properties such as cloud fraction and condensate mixing ratio, which are not reliably observed. Moreover, the simulated variables associated with the statistical properties of the clouds are internally consistent. On the other hand, CEMs do not explicitly resolve every scale of motions; they must have finer-scale parameterizations such as turbulence closure, cloud microphysics, and radiative transfer. CEMs have additional limitations, for example, the periodic lateral-boundary conditions. These limitations may or may not impact the simulated cloud-scale processes that have to be parameterized in an SCM. Thus, CEMs can be used as a valuable or complementary tool for SCMs to achieve the goal of improving cloud parameterizations in GCMs or numerical weather prediction models (Browning 1994; Randall et al. 1996).

Recently, Xu and Randall (1996; hereafter XR96) simulated the statistical behavior of tropical cumulus convection with Global Atmospheric Research Program (GARP) Atlantic Tropical Experiment (GATE) data, using a 2D CEM. The observed time variations of the

Corresponding author address: Dr. Kuan-Man Xu, Mail Stop 420, NASA Langley Research Center, Hampton, VA 23681-2199.
E-mail: k.m.xu@larc.nasa.gov

surface precipitation rate, surface evaporation rate, outgoing longwave radiation (OLR) flux, and the vertical distributions of temperature, water vapor mixing ratio, and relative humidity were successfully reproduced by the model, as were the vertical structures and time evolutions of the major convective systems. The simulated temperature and specific humidity departures from observations are generally small for most subperiods of the 18-day simulation (± 1 K and ± 1 g kg⁻¹), and seldom exceed 2 K and 1.5 g kg⁻¹, respectively. These results were obtained with the Thompson et al. (1979) dataset. Using the Ooyama (1987) dataset analyzed with a statistical interpolation scheme, the departures were further reduced, especially in the temperature and the specific humidity in the lower troposphere. In spite of this success, sensitivity tests in XR96 suggest that the 2D model has artificially strong inhibiting effects on convection and is unrealistically efficient in vertical transports of heat, moisture, and momentum when the vertical wind shear is strong. This deficiency of 2D models was noticed by Soong and Tao (1980), who reduced the upper-tropospheric wind shear by 20%. These limitations are expected to be amplified when applied to midlatitude convection because of the stronger, upper-tropospheric wind shear.

Shorter-term and longer-term simulations have also been performed in other groups individually or in an intercomparison mode with the GATE and Tropical Ocean Global Atmosphere Coupled Ocean–Atmosphere Response Experiment (TOGA COARE) datasets (Grabowski et al. 1996; Krueger 1997; Redelsperger et al. 2000; Li et al. 1999; Wu et al. 1998). Grabowski et al. (1996) produced similar magnitudes of temperature and specific humidity departures as in XR96. Systematic departures of -3 K and -1.5 g kg⁻¹ were, however, developed at the end of their 7-day simulation. Grabowski et al. attributed this to the lack of large-scale condensate forcing in the dataset. Using the same model as in Grabowski et al., Wu et al. (1998) performed a 38-day simulation with the TOGA COARE dataset. The simulated departures were slightly higher than those obtained with the GATE Phase III dataset (Grabowski et al. 1996). There was a systematic trend in the temperature and specific humidity departures, but with opposite signs ($+2$ to $+6$ K and $+4$ g kg⁻¹), for the last 10 days of the simulation. The quality of the TOGA COARE observations could be attributed to the larger departures, according to the intercomparison study of Krueger (1997) with a week-long simulation of TOGA COARE convection by eight CEMs.

Li et al. (1999) examined the impact of methods for imposing the large-scale advective tendencies (forcing methods) with the TOGA COARE dataset using the Goddard cloud ensemble (GCE) model; that is, the total advective forcing and the vertical flux forcing. The former prescribes the sum of the horizontal and vertical advective tendencies while the latter prescribes the large-scale vertical velocity and horizontal advective

tendencies. Li et al. (1999) found that the vertical flux forcing method produced smaller temperature and moisture departures than the total advective forcing method. They suggested that the adjustment of vertical thermodynamic structure to the imposed large-scale vertical velocity yields thermodynamic fields closer to the observed, especially in the temperature profiles. This conclusion, as shown in this study, may be premature; the quality of the datasets can alter such a conclusion.

None of the aforementioned studies dealt with the midlatitude continental convection using observed large-scale forcing data. Very short-term simulations of midlatitude squall lines/isolated clouds, without an explicitly imposed, observed large-scale forcing, were performed to compare the vertical structures of budget terms with their tropical counterparts (Schlesinger 1994) and the observed features of squall line structures (Tao et al. 1993) and to examine the mechanisms of cloud–radiation interactions (Tao et al. 1996).

It is well known that there are noticeable differences between the environments of the maritime tropical and midlatitude continental convective systems (e.g., Houze and Betts 1981; Houze and Hobbs 1982): 1) the underlying surface (oceans vs land), 2) the moisture content in the atmospheric column (wet vs dry), 3) the Rossby radius of deformation (large vs small), 4) the vertical shear of horizontal wind components (shallow vs deep layers), 5) the depth of the subcloud layers (shallow vs diurnally varying), 6) instability/inhibition (small vs large), and 7) the strength of horizontal advective tendencies of temperature and moisture (small vs large). Such differences manifest themselves in more complex and varied convective systems in midlatitude continental regions, but in many ways convective systems are rather similar between the two regions (Houze and Hobbs 1982).

Even though the structures, life cycles, and dynamic aspects of varieties of midlatitude continental convective systems have been extensively studied (e.g., Houze and Hobbs 1982; Johnson 1993), the interactions between cumulus convection and the large-scale midlatitude environment are far less well understood than in the maritime Tropics, due partly to fewer dedicated field experiments over long time periods and on synoptic scales. This poses a serious problem for developing cloud parameterizations and/or representations of cloud processes in GCMs in general because such parameterizations are based largely upon the understanding of cumulus–environment interactions over the tropical oceans.

There have been only a few studies focusing on the cumulus–environment interactions in the midlatitudes (e.g., Lewis 1975; Kuo and Anthes 1984; Ogura and Jiang 1985; Gallus and Johnson 1991; Grell et al. 1991; Wu 1993; Lin and Johnson 1994). Case studies were usually performed with observations of limited durations. For example, Lewis (1975) examined a prefrontal squall line case with the diagnostic cumulus ensemble

model of Ogura and Cho (1973). A main finding was that deep cumulus clouds are dominant in the diagnosed cloud spectrum. Kuo and Anthes (1984) used data (10–11 April 1979) from the Severe Environmental Storm and Mesoscale Experiment (SESAME), though of questionable quality, to examine the relative importance of individual terms in the heat and moisture budgets. They found that the vertical advection terms in the budgets are not as dominant as in the Tropics. Grell et al. (1991) semiprognostically tested three cumulus parameterization schemes with the same dataset: Arakawa and Schubert (1974), Kreitzberg and Perkey (1976), and Kuo (1974). Findings pertaining to the Arakawa–Schubert parameterization were 1) that the quasiequilibrium assumption is valid, and 2) that the inclusion of downdrafts is crucial to predict the cumulus feedbacks correctly. Such findings were confirmed by Wu (1993) with the dataset from the Oklahoma–Kansas Preliminary Regional Experiment for STORM-Central (OK PRE-STORM) project.

The OK PRE-STORM project in May and June 1985 provided an unprecedented high-resolution dataset for studying the detailed structures of mesoscale convective systems (MCS; Cunniff 1986). Gallus and Johnson (1991) and Lin and Johnson (1994) diagnosed the mesoscale budgets for two intense squall lines with weak (10–11 June 1985) and strong (26–27 June 1985) frontal forcings, respectively. They found distinct differences in the apparent heating source (Q_1) and apparent moisture sink [Q_2 ; see Yanai et al. (1973) for definitions] between convective and stratiform regions: single Q_1/Q_2 peaks in the convective regions but cooling/moistening (heating/drying) in the lower (upper) troposphere in the stratiform regions. The peak of Q_1 for the entire MCS was located in the middle/upper troposphere, while that of Q_2 varied greatly as the system became mature and decayed.

Ogura and Jiang (1985) simulated the statistical properties of an MCS using an idealized, steady forcing profile obtained during SESAME (10–11 April 1979) with a 2D CEM. A domain size of 128 km was used. The integration lasted for 17 h of physical time. Sporadic convection was produced even with a steady forcing, due to drying up of the subcloud layer and neglect of the surface fluxes. Other findings are that (i) the cloud population was dominated by deep clouds, and (ii) the convergences of the eddy heat and moisture transports were comparable to condensation and evaporation. There was, however, no observational data to evaluate the simulations due to their idealized nature. As mentioned earlier, Tao et al. (1993, 1996) simulated a PRE-STORM squall line (10–11 June 1985) with open lateral boundary conditions. Thus, no large-scale advective forcing could be imposed. At any rate, there has not been any other CEM study with observed midlatitude forcing data.

The present study also adopts a CEM as a tool to simulate the statistical properties of midlatitude cumulus

convection, but using time-varying observed large-scale advective tendencies over an 18-day period. Its major advantages relative to the Ogura and Jiang study include that 1) extensive observations are available to evaluate simulations; 2) observed surface fluxes are used to force the model; 3) more advanced model physics, such as ice-phase microphysics, turbulence closure, and radiative transfer parameterization, are included; and 4) a larger domain size is used.

The main objectives of this study are: (i) to evaluate the performance of the CEM against midlatitude observations, and (ii) to examine the similarities and differences of midlatitude and tropical cumulus convection in terms of the statistical properties of cumulus ensembles. Such a comparison for updraft and downdraft statistics has been presented in Xu and Randall (2000, submitted to *J. Atmos. Sci.*). To achieve the second objective, some results for tropical convection from XR96 will be used in the present study.

2. Numerical simulation

The model used in this study is the 2D University of California at Los Angeles–Colorado State University (UCLA-CSU) CEM. The details of the CEM have been described by Krueger (1988), Xu and Krueger (1991), and Xu and Randall (1995). Briefly, the dynamics of the CEM is based on the anelastic system. The v -momentum equation is also included due to the inclusion of the Coriolis acceleration. The physical parameterizations in the model consist of 1) a third-moment turbulence closure (Krueger 1988), 2) a three-phase bulk cloud microphysics (Lin et al. 1983; Lord et al. 1984; Krueger et al. 1995a), and 3) an interactive radiative transfer (Harshvardhan et al. 1987; Xu and Randall 1995). The third-moment turbulence closure consists of 35 prognostic equations for second and third moments, and a diagnostic equation for the turbulent length scale. The interactive radiative transfer parameterization is based on Harshvardhan et al.'s (1987) broadband radiative transfer model with cloud optical properties as formulated by Stephens et al. (1990).

Some aspects of the design of simulations that may impact the simulated results are (i) the periodic lateral-boundary conditions, (ii) the zero terminal velocity for cloud ice crystals, (iii) the lack of large-scale horizontal advection of condensate, (iv) the omission of a turbulence-scale cloudiness parameterization, (v) the method of prescribing large-scale advective tendencies, and (vi) the way of nudging the simulated, domain-averaged horizontal wind components toward the observed winds. These aspects have been discussed by XR96.

As with single-column models (Randall et al. 1996), the horizontally uniform, large-scale, horizontal advective cooling and moistening rates and vertical velocity or the total advective tendencies are prescribed in each simulation. Another variable prescribed in the CEM is the large-scale horizontal pressure gradient; the ob-

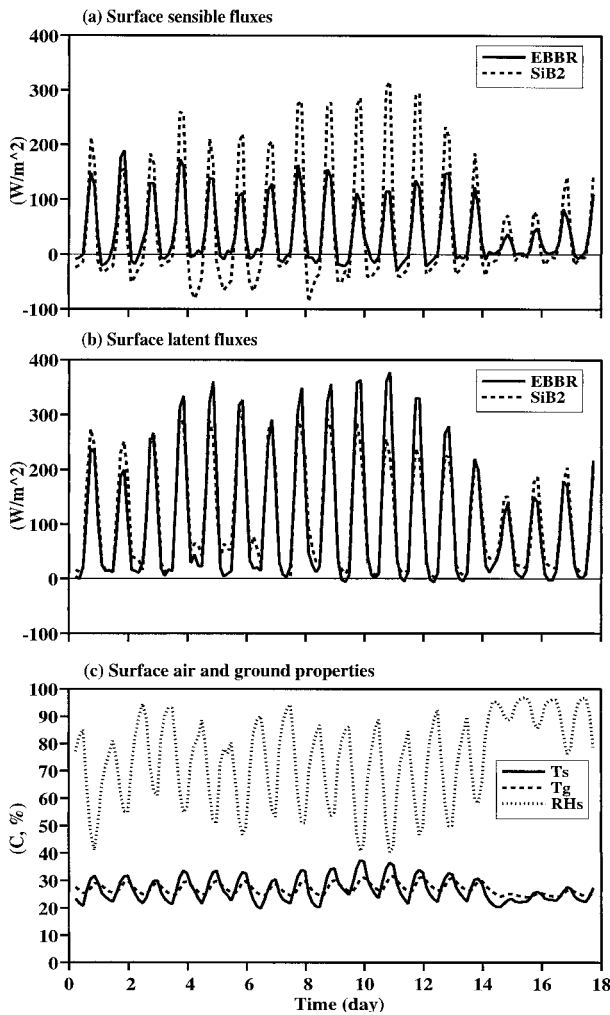


FIG. 1. The time series of EBBR-observed and SiB2-calculated (a) surface sensible and (b) latent heat fluxes, as well as (c) observed surface air temperature, ground temperature, and surface relative humidity during the 18-day IOP starting from 0000 UTC 18 Jul 1995.

served wind components are used to approximate the large-scale horizontal pressure gradients through the geostrophic wind relation due to the lack of observed data. This is merely consistent with the dynamic framework mentioned above (Xu and Krueger 1991). A nudging procedure is used so that the domain-averaged horizontal wind components are approximately equal to the observed ones, with a nudging time of 1 h (XR96). The horizontal inhomogeneity of u and v inside the CEM domain is, however, preserved by the nudging procedure.

Many other aspects of the ARM simulations described below are identical to the GATE simulation performed by XR96 except that the surface sensible and latent heat fluxes are prescribed in the model, based on either Energy Balance/Bowen Ratio (EBBR) observations at the ARM Southern Great Plain (SGP) Cloud and Radiation Testbed (CART) sites or those calculated using the Sim-

TABLE 1. Results of sensitivity simulations. See text for explanation.

Forcings	Simulation	MTA	MQA	MPA	MTC	MQC	MPC
LLNL-	A	1.88	1.92	0.69	0.41	0.64	0.72
EBBR	B	1.66	1.58	0.63	0.48	0.67	0.61
	C	0.57	0.70	0.40	0.84	0.77	0.67
SUNY-	D	1.37	1.07	1.15	0.32	0.57	0.82
EBBR	E	1.34	1.04	1.19	0.54	0.67	0.78
	F (not run)						
SUNY-	D2	1.06	1.04	1.03	0.58	0.63	0.82
SiB2	E2	1.27	1.11	1.20	0.62	0.67	0.82
	F2	1.16	0.80	1.00	0.67	0.78	0.73

ple Biosphere Model Version 2 (SiB2; Sellers et al. 1996; Doran et al. 1998; see Figs. 1a and 1b). It should be emphasized that this procedure only restrains the CEM domain-averaged surface heat fluxes, not those at individual grid points. As in the GATE simulations, the surface heat fluxes at individual grid points are calculated using the bulk aerodynamic formula to retain the horizontal inhomogeneity of the surface heat fluxes, which may impact continental convection. A climatological value of the wetness parameter, 0.15, is used in the formula.

Eight simulations have been performed with the July 1995 IOP data in this study. Results from one simulation (D2) are extensively presented and compared with observations, while those of other simulations are briefly presented. Simulation D2 uses the advective forcing data analyzed at the State University of New York (SUNY), Stony Brook (Zhang and Lin 1997) with the SiB2-calculated surface fluxes. The analyzed dataset will be discussed in section 3. The large-scale total advective tendencies are prescribed in the model for simulation D2. The naming of the simulation follows the single-column model (SCM) intercomparison study (Ghan et al. 2000), in which the UCLA-CSU CEM is one of the participants. The main reason for comparing D2 results with observations is because it is the baseline simulation in the intercomparison study and its overall results agree most favorably with the available observations (Table 1).

As discussed by XR96, an ensemble of experiments with slightly different initial conditions should be performed to obtain an ensemble mean of experiments for a given simulation. Such an ensemble of experiments is computationally expensive because eight simulations are performed. Therefore, this study performs only one experiment for each simulation. Uncertainties in observations and analyses could, as discussed later, be likely to alter the results more than the lack of enough realizations.

The remaining aspects of the simulations are identical to those described in earlier studies with the UCLA-CSU CEM (Xu and Krueger 1991; Xu et al. 1992; Xu and Randall 1995; XR96). For example, the domain size is 512 km, with a horizontal grid size of 2 km. The vertical coordinate is stretched to give finer resolution

near the surface (~ 100 m), with 33 layers. The radiation module is called every 150 s using the “accumulated” method proposed by Xu and Randall (1995).

3. The IOP dataset

The July 1995 IOP covers an 18-day period, starting from 0000 UTC 18 July and ending at 2300 UTC 4 August. Balloon-borne soundings of winds, temperature, and dewpoint temperature are obtained every 3 h from the CART central facility located near Lamont, Oklahoma (36.61°N , 97.49°W), and from four boundary facilities [Morris, Oklahoma (35.69°N , 95.86°W); Purcell, Oklahoma (34.97°N , 97.42°W); Vici, Oklahoma (36.07°N , 99.22°W); and Hillsboro, Kansas (38.31°N , 97.30°W)], which form a rectangle of approximately $300\text{ km} \times 370\text{ km}$. Hourly wind data from 17 profilers surrounding the CART array are also available as additional inputs for the constrained variational objective analysis performed at SUNY (Zhang and Lin 1997). This analysis provides a dynamically and thermodynamically consistent dataset in terms of vertically integrated quantities, that is, the mass, energy, moisture, and momentum budgets, with adjustments in the dry static energy, water vapor mixing ratio, and the horizontal wind components not far exceeding the uncertainties of the original measurements. The amount of the adjustments in this version of the dataset (Zhang 1998) was assumed to be height independent. This may have slight impacts on the analyzed advective tendencies imposed in the model.

Additional procedures such as a scale-controlled statistical interpolation similar to that of Ooyama (1987) were also implemented in the preprocessing of data. All surface constraint variables, for example, surface heat fluxes and radiative fluxes, are first gridded and then areally averaged. Measurements from a variety of platforms such as the sondes, surface meteorological observation system (SMOS), EBBR, and Oklahoma (OK) Mesonet and Kansas Mesonet were merged to produce the surface composites for the variational analysis. There are two versions of the SUNY analyses, one with the EBBR surface heat fluxes and the other with the SiB2 surface heat fluxes (Figs. 1a and 1b). The SiB2 fluxes-based analysis is used in the baseline simulation. The differences of the EBBR and SiB2 surface heat fluxes are due mainly to the locations of EBBR stations restricted to pasture and areas of natural vegetation rather than cultivated fields. The cultivated fields in summer can be expected to have higher sensible heat fluxes and lower latent heat fluxes than areas occupied by EBBR stations (Doran et al. 1998).

The observed time–height cross sections of temperature and water vapor mixing ratio for the July 1995 IOP are shown in Fig. 2. The observed temporal variation of the temperature is relatively small in the middle and upper troposphere but is very large near the surface (Fig. 2a), with a predominant diurnal cycle (also see

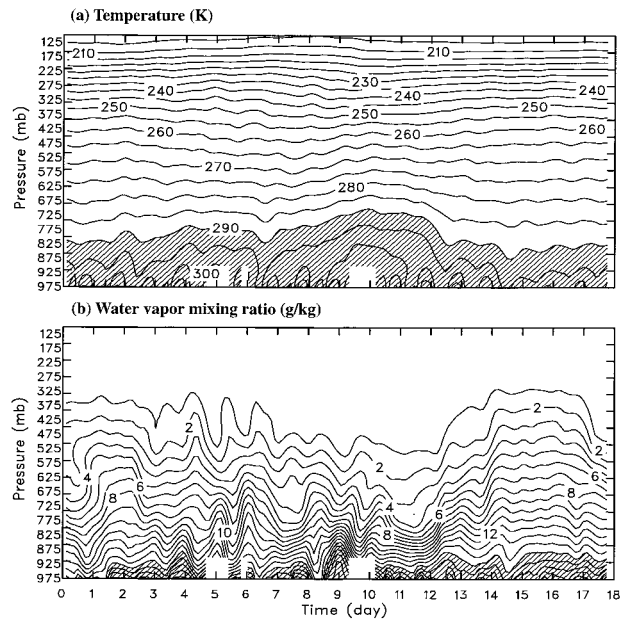


FIG. 2. Time–height cross sections of the observed (a) temperature and (b) water vapor mixing ratio for the Jul 1995 IOP. The contour interval is 5 K in (a) and 1 g kg^{-1} in (b). Temperatures over 290 K are hatched in (a), while water vapor mixing ratios over 15 g kg^{-1} are hatched in (b).

Fig. 1c). This is typical of midlatitude continental conditions, which are drastically different from those of the maritime Tropics. On the other hand, the observed water vapor mixing ratio undergoes great variations throughout the troposphere during the 18-day IOP (Fig. 2b). There is a dry subperiod in the middle of the IOP. The diurnal variations of near-surface moisture are very large at the SGP CART site (Fig. 2b). This is related to the large variations of surface latent heat fluxes (Fig. 1b), with diurnal amplitudes of $200\text{--}350\text{ W m}^{-2}$. The diurnal amplitudes of sensible heat fluxes are slightly smaller than those of latent heat fluxes. Such large variations of surface turbulent fluxes are not normally observed over the tropical oceans.

The horizontal wind speed is large in the upper troposphere (Figs. 3a and 3b). Vertical wind shear is frequent, with its maximum in the middle-to-upper troposphere. This differs from the Tropics where low-level wind shear is more typically observed, which is associated with the occurrence of the easterly jets. On the other hand, the vertical velocity (Fig. 3c) exhibits pronounced temporal variations; 1) bidiurnal variations during the first 9 days, 2) relatively undisturbed from days 10 to 14, and 3) rather disturbed at the end of the IOP. That is, the entire IOP is convectively active except for the middle subperiod (Fig. 4a).

Horizontal advective coolings with magnitudes of $5\text{--}10\text{ K day}^{-1}$ are observed in the middle and upper troposphere during the first 10 days, while a large advective warming appears in the lower troposphere on days 8 and 9 (Fig. 5a). Surprisingly, there is little hor-

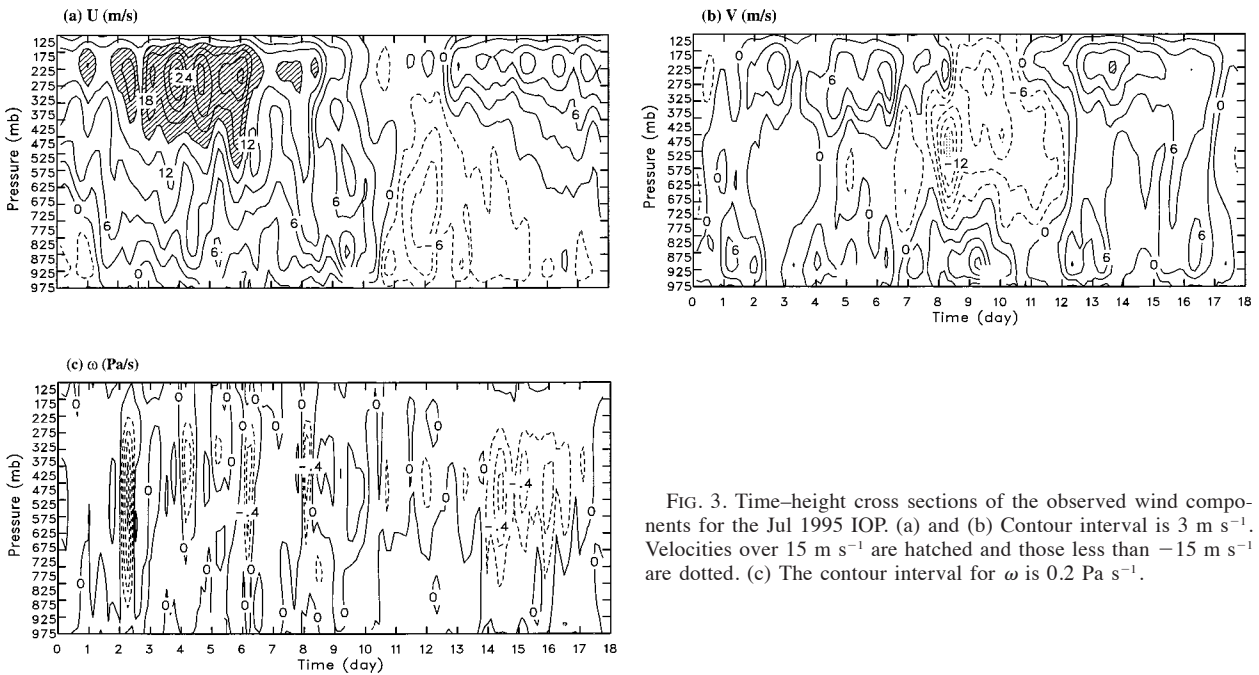


FIG. 3. Time–height cross sections of the observed wind components for the Jul 1995 IOP. (a) and (b) Contour interval is 3 m s^{-1} . Velocities over 15 m s^{-1} are hatched and those less than -15 m s^{-1} are dotted. (c) The contour interval for ω is 0.2 Pa s^{-1} .

horizontal advective cooling in the lower and middle troposphere during the last 5 days of the IOP when cumulus convection is active (Fig. 4a), suggesting that convection is locally generated.

Generally, horizontal advective moistenings have more complicated patterns of variations with magnitudes of $3\text{--}6 \text{ g kg}^{-1} \text{ day}^{-1}$ during the early portion of the IOP (Fig. 5b). Comparison with the observed surface precipitation (Fig. 4a) shows that advective moistening precedes and/or coincides with a precipitation event, while advective drying usually appears after a precipitation event. Synoptic summary indicates that there were frontal passages during the early portion of the IOP. Nevertheless, such a phase relationship reveals that the horizontal moisture advection plays a more important role in midlatitude convection than the horizontal temperature advection. A strong drying with a magnitude of over $10 \text{ g kg}^{-1} \text{ day}^{-1}$ occurs on days 9 and 10 and is responsible for a strong decrease of moisture (Fig. 2b). On days 12 and 13, a very strong advective moistening with a magnitude of about $9 \text{ g kg}^{-1} \text{ day}^{-1}$, builds up the moisture before a strong convective event occurs.

The total advective cooling and moistening, which include the horizontal and vertical advective tendencies (Figs. 5c and 5d), are matched to the observed precipitation events well (Fig. 4a). The strong precipitation events (days 3, 7, 9, and 15–17) are associated with strong total advective cooling and moistening. The maximum total advective cooling centers are located slightly above the middle troposphere, while the maximum total advective moistening centers are located near the middle troposphere. Moreover, total advective moistening is rather weak during the weak precipitation events (days

4–6), while total advective cooling is aloft. These high and aloft maximum centers are significantly different from those observed in the Tropics where the maximum centers are located in the lower and middle troposphere.

4. Results

a. Basic features of the simulated convection

Based on the Hovmöller diagrams (x – t sections) of surface precipitation rate and OLR flux (Figs. 6 and 7), the simulated cloud systems during the five major precipitation events can be classified as: 1) quasi-stationary on day 3; 2) propagating (eastward) squall-type on days 5, 7, and 9, lasting for 6–8 h; and 3) weakly organized and short lived (at least, from surface precipitation; but high clouds last longer) from days 14 to 18, which is related to the weak vertical wind shear (Fig. 3). The weak precipitation event on day 4 is, however, not well simulated (not shown).

The precipitation events on days 3, 5, 7, and 9 occur during local evenings when the surface turbulence fluxes are small. The nocturnal nature of these cloud systems is typical of the SGP region (Cunning 1986). For the squall-type MCSs on days 7 and 9, the horizontal extents of surface precipitation do not change much with time although the OLR shows an increase of horizontal extent as the MCSs decay (Figs. 7b and 7c). The main difference between days 7 and 9 is that the MCS on day 7 is more continuous. The short life cycle (<12 h) of these MCSs is related to their rapid passage across the SGP CART domain.

Another feature seen in Figs. 6 and 7 is that midlat-

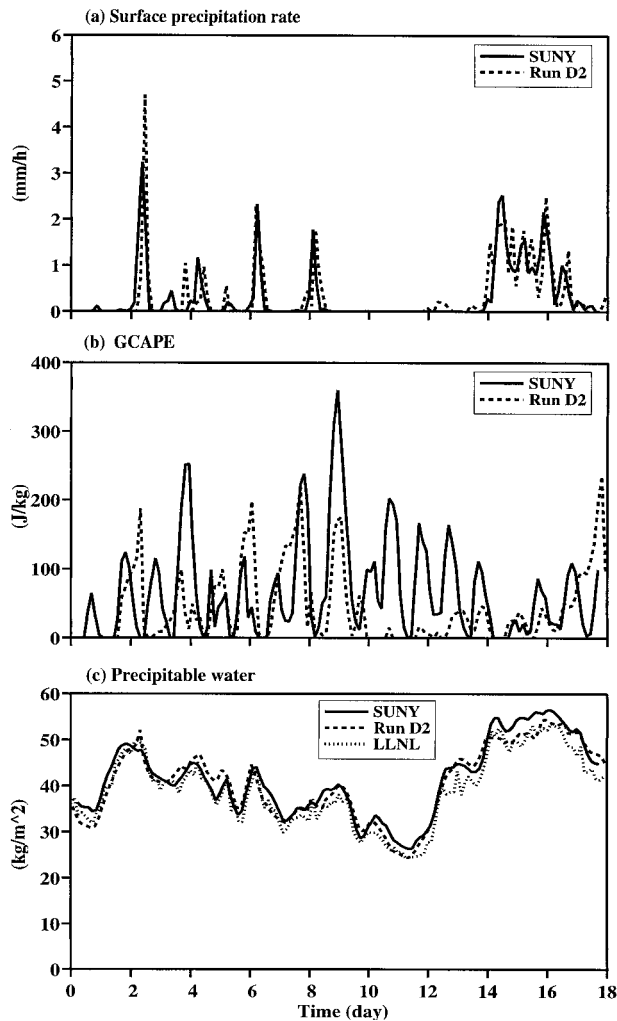


FIG. 4. Time sequence of domain-averaged (a) surface precipitation rates, (b) generalized convective available potential energy (GCAPE), and (c) precipitable water for simulation D2 and observations. (c) Two versions of the analyzed soundings are used to calculate the precipitable water by the State University of New York (SUNY) and the Lawrence Livermore National Laboratory (LLNL) groups, respectively.

itude convection is more rapidly developed than its tropical counterpart. That is, convection immediately reaches its peak intensity once it overcomes convective inhibition, perhaps due to much stronger, initial convective instability in midlatitudes. Afterward, weakly organized systems tend to decay quickly, as far as the surface precipitation is concerned, for example, on day 16 (Fig. 6d). Such short longevity of cloud systems is often observed in the midlatitude summer.

In general, the direction of propagation of simulated cloud systems is controlled by the lower-tropospheric winds (Fig. 6). The upper-level anvil clouds follows the upper-tropospheric winds (Fig. 3a). The slow decay of the anvil clouds suggests that anvil clouds are advected

by the mean winds, especially for the weakly organized systems (Fig. 7d).

b. Sensitivity simulations

There are three sets of simulations performed in this study, with slightly/significantly different imposed large-scale advective forcings and/or surface sensible and latent heat fluxes (Table 1). Within each set, different methods of imposing the large-scale advective forcings are used, that is, the total advective tendencies (A, D, and D2), the horizontal advective tendencies plus the large-scale vertical velocity (B, E, and E2), and the relaxation forcing (C, F, and F2). Randall and Cripe (1999) described the details of the relaxation method and examined the strengths and weaknesses of each method with a single-column model.

The imposed large-scale advective forcings are significantly different between the traditional objective analysis performed at the Lawrence Livermore National Laboratory (LLNL; Leach et al. 1996) and the constrained variational analysis performed at SUNY (Zhang and Lin 1997). The differences between the last two sets of simulations shown in Table 1 are associated mainly with the surface sensible and latent heat fluxes.

To concisely present the sensitivity results, a set of nondimensional figures of “merit” is presented, as in Randall and Cripe (1999):

- MTA: the vertical mass integral of the root-mean-square (rms) temperature errors, normalized by the vertically integrated temporal standard deviation of the temperature;
- MTC: the vertical mass integral of the temporal correlation coefficient between the simulated and observed temperatures;
- MQA: same as MTA except for the water vapor mixing ratio;
- MQC: same as MTC except for the water vapor mixing ratio;
- MPA: the ratio of the simulated and observed time-averaged surface precipitation rates; and
- MPC: the temporal correlation of the simulated and observed surface precipitation rates.

In a perfect simulation, MTA and MQA will be equal to zero, while the other four figures will be equal to one. An obvious conclusion from Table 1 is that none of the simulations is close to being perfect.

It is also apparent that the differences are the greatest between the LLNL and SUNY forcings: MTA and MQA from A and B are much greater than those in D, E, D2, and E2, while the mean surface precipitation rates are significantly underestimated in A and B, which is related to much drier, simulated atmosphere (not shown) as a result of larger advective drying rates during some convectively inactive subperiods than in the SUNY analyses. Another conclusion is that simulations with the Sib2 fluxes are slightly better than those with the EBBR

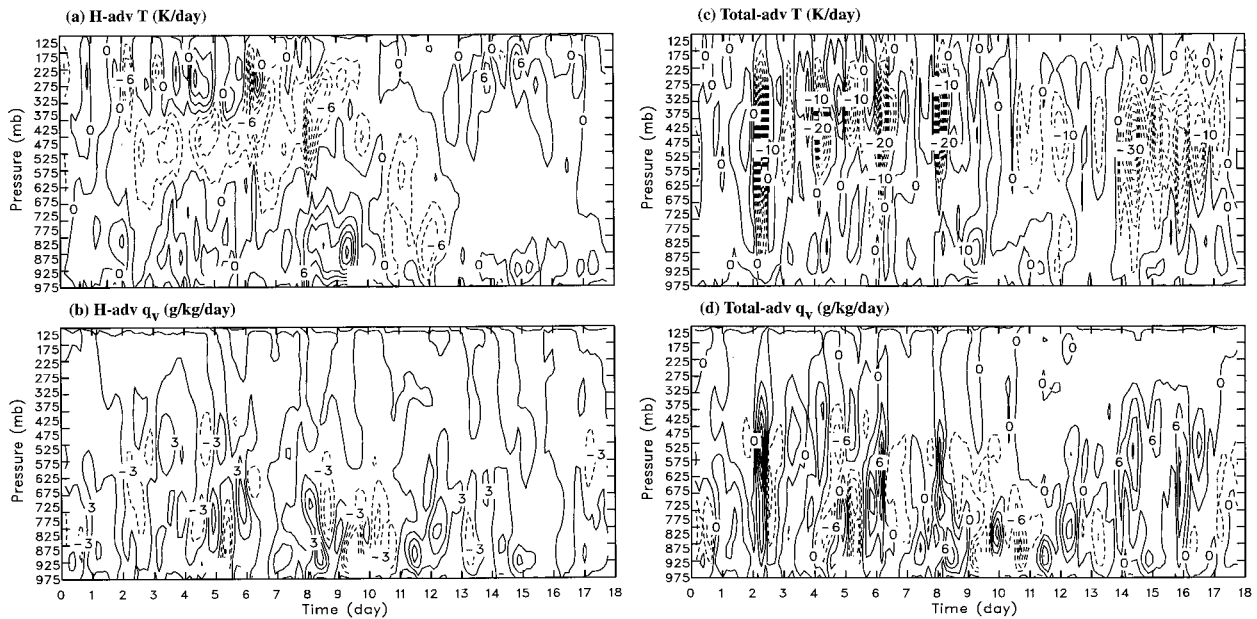


FIG. 5. Time–height cross sections of the observed horizontal and total advections of temperature and moisture for the Jul 1995 IOP. The contour interval is (a) 3 K day^{-1} , (b) $3 \text{ g kg}^{-1} \text{ day}^{-1}$, (c) 5 K day^{-1} , and (d) $6 \text{ g kg}^{-1} \text{ day}^{-1}$.

fluxes from the comparison of all figures of merit between the second and third sets of simulations, with greater improvement in D2 than in E2. In addition, the vertical flux method (B, E, and E2) does not produce better results than the total forcing method (A, D, and D2). This differs from the conclusion drawn by Li et al. (1999), based upon week-long TOGA COARE simulations.

Run C shows much smaller MTA and MQA, and much higher MTC and MQC than the nonrelaxation runs (A and B). That is, the simulated soundings are closer to the observed, as expected, due to relaxation to the observed temperature and moisture profiles. The mean surface precipitation rate is, however, significantly underestimated because convective circulations are destroyed by the strong relaxation effects in the form of artificial advective tendencies, which are large enough to cancel the observed advective tendencies during some subperiods so that convection cannot last long. A much better mean precipitation rate but larger MTA and MQA are produced in run F2 than in run C because the relaxation timescales used in run F2 are four times bigger than the “diagnosed” advective timescales, which allows convective circulations to be developed with smaller relaxation effects. Reducing the relaxation timescales yields similar results as in run C (not shown).

c. Thermodynamic properties

All of the simulated variables shown below are averaged over the entire domain in space and over 3 h in time from the baseline simulation D2. That is, the tem-

poral averaging interval is identical to that used in observations.

The temperature and moisture differences between simulation D2 and observations for the July 1995 IOP are shown in Fig. 8. Typical temperature differences are between -2 K and $+2 \text{ K}$ in the troposphere during the IOP, with the smallest differences appearing in the convectively active portions of the IOP. The standard deviations of the observed temperature (Fig. 9b), which measures the observed variabilities, are about 1.5 K in the middle and upper troposphere and $3\text{--}4 \text{ K}$ in the lower troposphere. Thus, the temperature differences shown in Fig. 8a are close to the observed variabilities for large portions of the IOP (also see Table 1). They are indeed slightly larger than those for the GATE simulations (XR96). Note that the observed variabilities of the maritime tropical atmosphere are less than 1 K . Therefore, the simulated temperature for D2 is acceptable, relative to the observed variabilities of the midlatitude atmosphere.

The largest temperature differences ($>4 \text{ K}$) between simulation D2 and observations appear in the low and upper troposphere from days 10 to 14. This feature also appears in other CEM and SCM simulations (D, E, and E2; Ghan et al. 2000) performed with data from the variational analysis, but with larger magnitudes. Uncertainties in observations on day 10 are the probable cause (M.-H. Zhang 1997, personal communication).

The differences between the simulated and observed water vapor mixing ratios (Fig. 8b) are generally smaller in the middle and upper troposphere than the observed variabilities (Fig. 9c) for large portions of the IOP. The

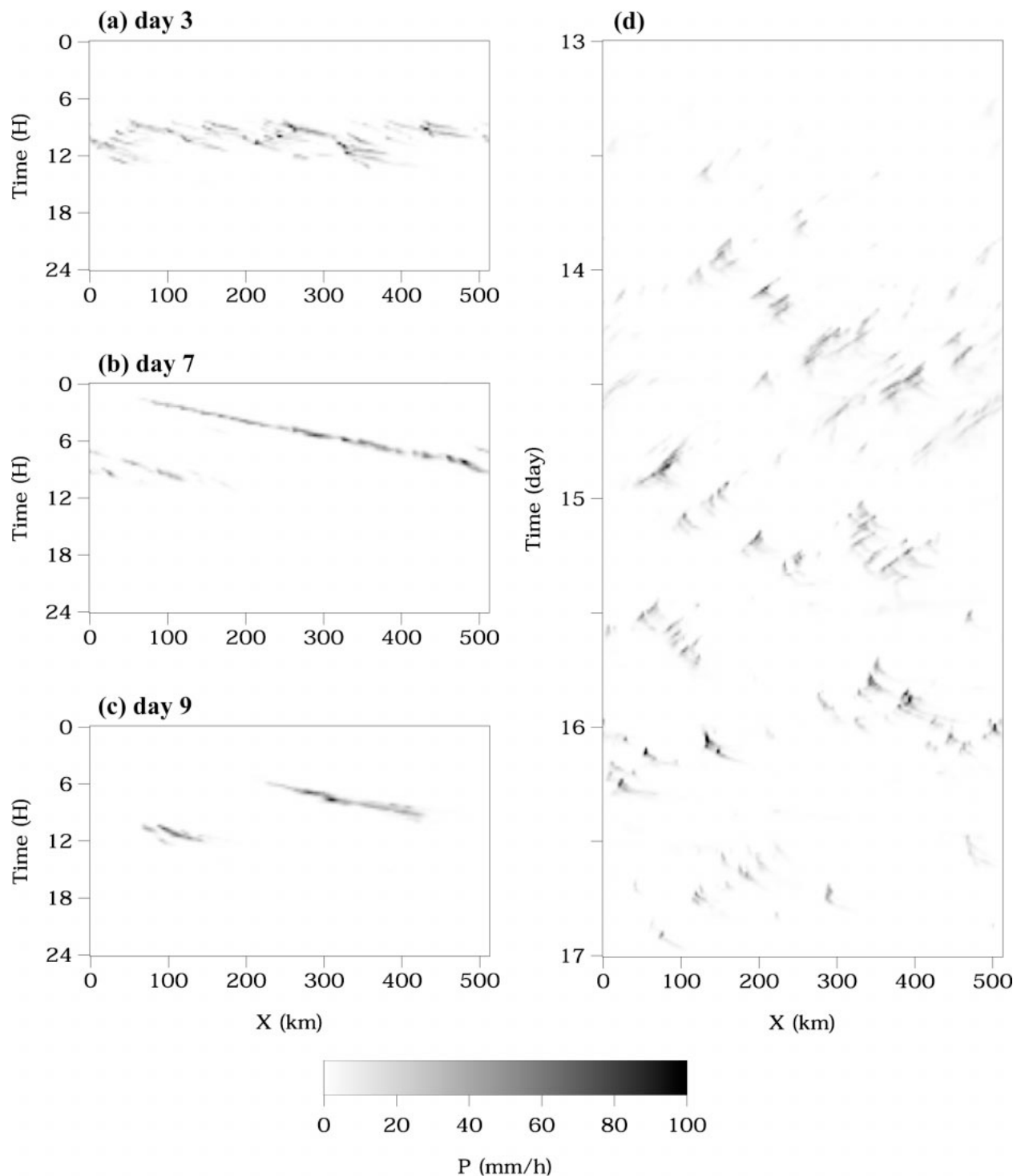


FIG. 6. Hovmöller diagrams ($x - t$ sections) of surface precipitation rate for four selected periods of simulation D2. A linear gray scale is used: white for zero and black for over 100 mm h^{-1} .

simulated lower troposphere is more humid than observed before and during the early hours of the precipitation events for the early portion of the IOP, due to delayed development of convection. The largest differ-

ences appear between days 9 and 14, with drier atmosphere below 800 mb and moister atmosphere between 800 and 450 mb. The reason for this can be related to the observed total moisture advective tendencies be-

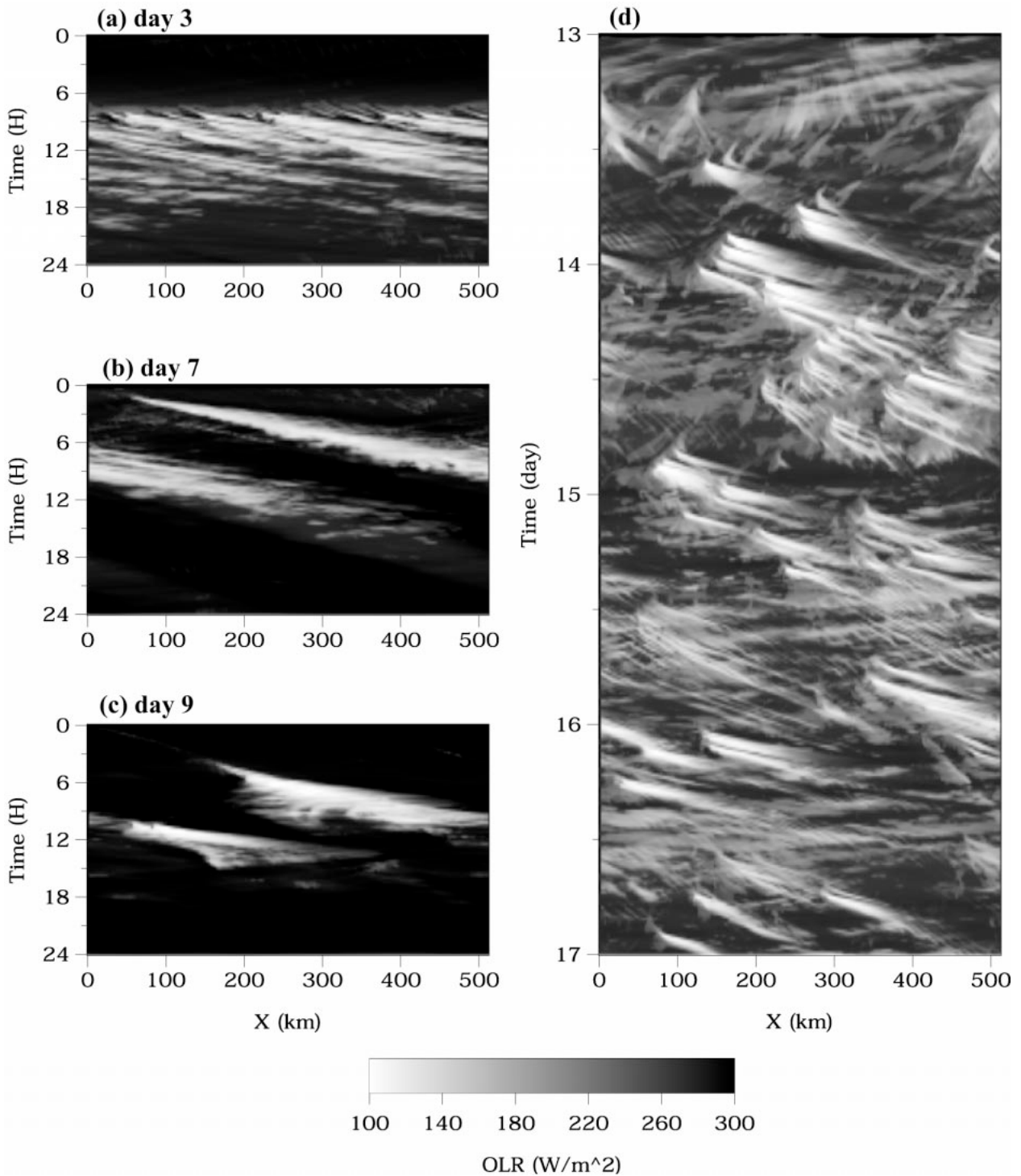


FIG. 7. Same as Fig. 6 except for OLR fluxes. A linear grayscale is used: white for less than 100 W m^{-2} and black for over 300 W m^{-2} .

cause such large differences also appear in other simulations (D and E) performed with the EBBR fluxes-based analysis (not shown). Inspection of the total moisture advective tendencies (Fig. 5d) does reveal 1) that

there is large advective drying ($>9 \text{ g kg}^{-1} \text{ day}^{-1}$) below 800 mb on both days 10 and 11, which may be excessive; and 2) that there is rather weak advective drying above 800 mb where the observed moisture also de-

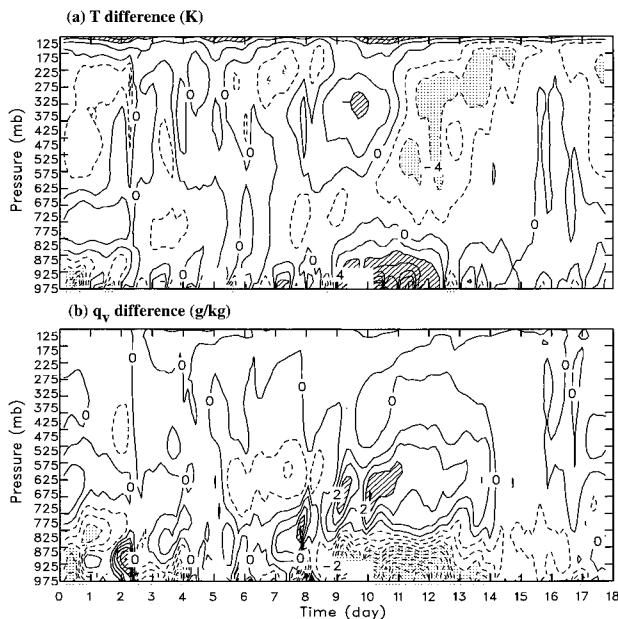


FIG. 8. Time–height cross sections of (a) the temperature difference and (b) the water vapor mixing ratio difference between simulation D2 and observations. The contour interval is 2 K in (a) and 1 g kg^{-1} in (b). Contours over 4 K (3 g kg^{-1}) are hatched. Contours less than -4 K (-3 g kg^{-1}) are dotted.

creases with time (Fig. 2b), which does not provide enough drying effects so that positive biases occur in all simulations.

Another feature in Fig. 8b is that the moisture differences are smaller than the observed variabilities (Fig. 9c) during the last precipitation event of the IOP, which coincides with the negligible temperature differences (Fig. 8a). These results suggest that the model produces more realistic results for the precipitating events with little large-scale horizontal advection (Fig. 5). When the horizontal temperature and/or moisture advective tendencies are large, the simulated temperature and/or moisture deviate greatly from the observed. This suggests that the lack of accurate measurements of the horizontal temperature and moisture advective tendencies in midlatitudes are the probable cause for the large temperature and moisture differences. Another probable cause is the lack of measurements of the large-scale horizontal advection of condensate. This is difficult to judge by looking at the moisture differences alone (Fig. 8b). It may be that in the configuration used, the model cannot produce realistic simulations under conditions of strong forcings due to horizontal advection because under these conditions more than the horizontal advective tendencies of temperature and water vapor are required. In addition, under such conditions, a single realization may not be adequate, due to stochastic nature of MCSs, as shown by Xu et al. (1992) and XR96.

The large departures of the simulated temperature and moisture from observations have a great impact on the instability of the atmosphere, for example, as measured

by a generalized convective available potential energy (GCAPE; Fig. 4b), following the computational procedure of Wang and Randall (1994). Fortunately, the largest differences between observed and simulated GCAPEs appear mainly during convectively inactive portions of the IOP, especially between days 9 and 14. The simulated mean (standard deviation) of the GCAPE is 44 J kg^{-1} (53 J kg^{-1}), compared to the observed mean (standard deviation) of 54 J kg^{-1} (61 J kg^{-1}) for convectively active portions of the IOP, where convectively active periods are defined by *observed* surface precipitation rates being greater than 0.1 mm h^{-1} . For convectively inactive portions of the IOP, however, the mean of simulated GCAPE (44 J kg^{-1}) is much smaller than that of the observed (80 J kg^{-1}), especially between days 9 and 14. The underestimate is related to the drier lower troposphere and the moister middle troposphere (Fig. 8b). Nevertheless, the model somewhat captures the large variabilities of the GCAPE in midlatitudes, but with less accuracy than in the Tropics (XR96).

A concise, statistical description of the differences between simulation and observation is presented with the temporal correlation coefficient and the rms errors, as well as the temporal standard deviations of observed and simulated profiles (Fig. 9; Table 1). The temporal correlation coefficients between the simulated and observed temperature and moisture are positive at all levels, with the highest values in the lowest troposphere for both temperature and moisture and in the upper troposphere for moisture only (Fig. 9a). The large temperature errors between days 9 and 14 (Fig. 8a) are responsible for the low temporal correlation in the upper troposphere.

The rms error of temperature is about 1 K near 800 mb, which coincides with a correlation coefficient of 0.95. The rms errors of the temperature are basically smaller (slightly larger) than the observed standard deviations in the lower (upper) troposphere (Fig. 9b). The rms errors of the moisture are smaller than the observed standard deviations at all levels except below 800 mb (Fig. 9c). Larger rms errors near the surface suggest that it is more difficult to simulate the subcloud layers over land than over oceans due to stronger variations of their thermodynamic structures over land and due to prescribing the surface heat fluxes.

Another statistical comparison is made in terms of the apparent heat source (Q_1) and apparent moisture sink (Q_2), which measure cumulus heating and drying, respectively [see Yanai et al. (1973) for definitions]. Only convectively active subperiods are included in the calculation because convectively inactive subperiods do not contribute to Q_1 and Q_2 . The temporal correlation coefficients are very high (0.70 for Q_1 and 0.80 for Q_2), except for the lowest 200 mb (Fig. 9d). The high correlation is not surprising because the small temporal correlation indicates that the simulated temporal tendencies differ from those observed because the observed total advective tendencies are included in both simulated and observed Q_1 and Q_2 . The simulated profiles of tem-

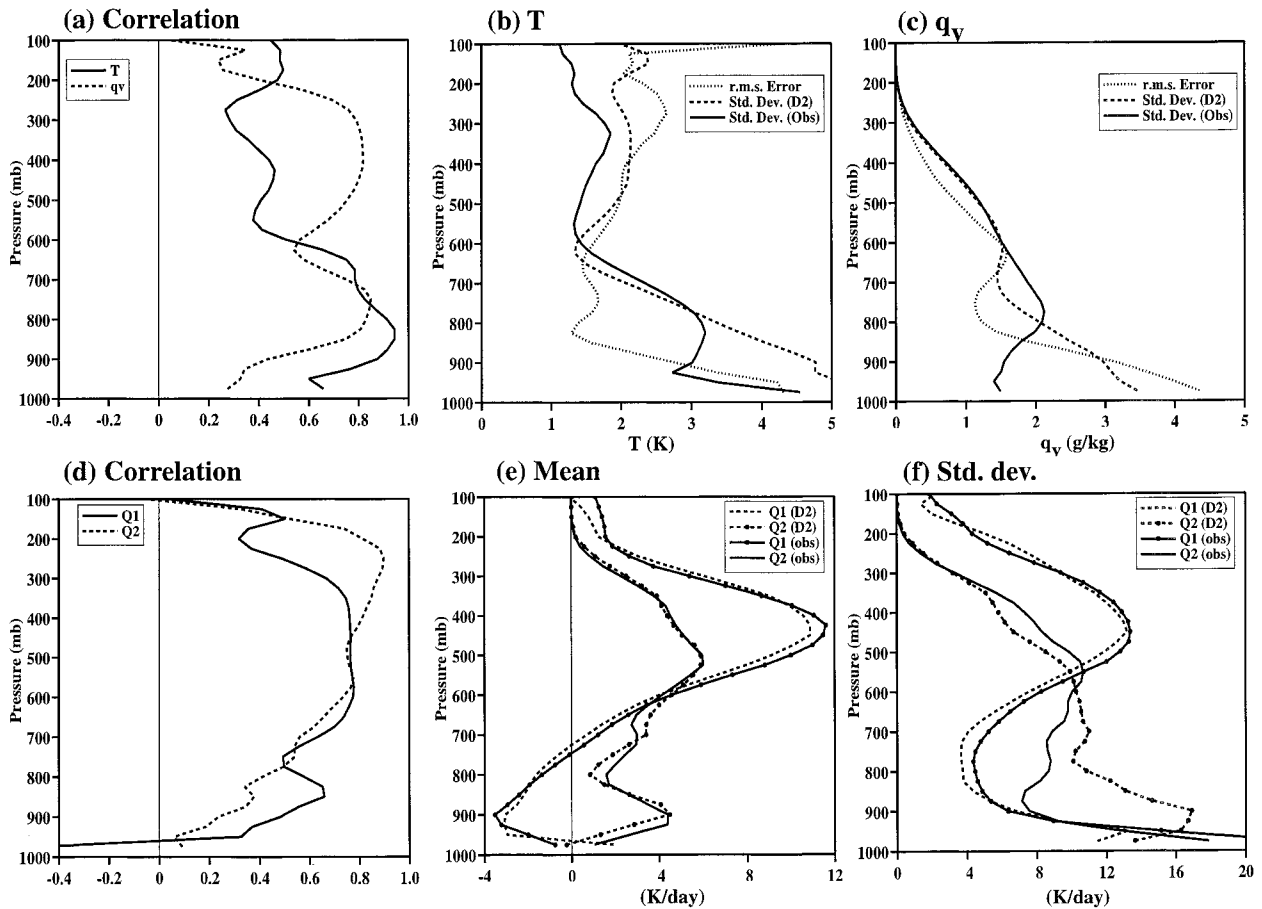


FIG. 9. The vertical profiles of (a) temporal correlation coefficient between simulated and observed temperature and moisture, (b) temperature, and (c) moisture rms errors and standard deviations. (c) The vertical profiles of temporal correlation coefficient, (d) mean and standard deviations of apparent heat source (Q_1), and (e) apparent moisture sink (Q_2) of simulation D2 and observation.

poral means (Fig. 9e) and standard deviations (Fig. 9f) of Q_1 and Q_2 are similar to the observed except for the larger standard deviations of Q_2 in the lower troposphere, which are related to the large moisture biases shown in Fig. 8b.

The vertical structures of the mean Q_1 and Q_2 profiles show the following features: 1) a maximum at 400 mb and a minimum at 900 mb in Q_1 , and 2) double maxima at 900 mb and 500 mb in Q_2 . Such vertical structures differ significantly from those in the Tropics (e.g., Yanai et al. 1973; Cheng 1989) and those of a simulated PRE-STORM squall line (Tao et al. 1993), but are rather similar to those of an observed PRE-STORM squall line (e.g., Gallus and Johnson 1991); that is, (i) apparent cooling below 750 mb, (ii) large apparent drying around 500 mb, and (iii) higher locations of Q_1 and Q_2 maxima. Such differences are probably due to the land–ocean differences and the differences between tropical and midlatitude large-scale dynamics. For example, the lower troposphere in midlatitudes is slightly drier, which is favorable for evaporation of rainwater; that is, producing cooling and moistening.

Next, the domain-averaged precipitable water is examined (Fig. 4c). The simulated precipitable water is within the uncertainties of data analyses. No significant differences from observations are noticed in Fig. 4c. The domain-averaged surface precipitation rates agree very well with observations (Fig. 4a). All major precipitation events are well captured in terms of their magnitudes (except for day 3) and timing. The minor precipitation events on day 4 are not reproduced, but high clouds were present (shown later). A false, weak precipitation event was simulated on day 13. Based upon the observed total advective tendencies, it is not surprising to see such a precipitation event (Fig. 5). A careful examination of Fig. 4a also reveals that there is a phase delay of the precipitation event on day 9, which can also be expected by examining the observed total advective tendencies.

d. Cloud characteristics

A comparison between observed and simulated liquid water paths during the IOP is shown in Fig. 10a. There

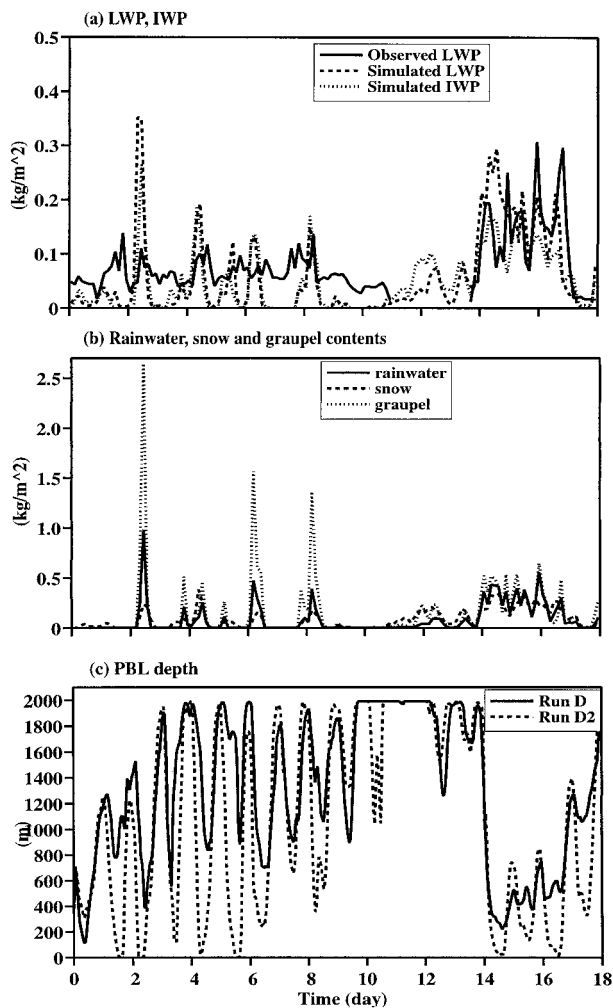


FIG. 10. Time sequence of domain-averaged (a) simulated (D2) and observed liquid water paths (LWPs) and ice water path (IWP); and (b) simulated (D2) rainwater content, snow content, and graupel content; and (c) planetary boundary layer (PBL) depths from D and D2.

were no measurements between days 11 and 14. There is a qualitative agreement between observation and simulation, due partly to an uncertainty of 0.03 kg m^{-2} associated with the microwave radiometer measurements (Liljegren 1994) and to the absence of low LWPs during convectively inactive portions of the IOP. That is, some low-level thin clouds are not simulated by the model. The agreement is, however, especially good during the last convectively active subperiod between days 15 and 17.

The ice water path and the vertically integrated amounts of snow, rainwater, and graupel are also shown in Fig. 10b, but their observational counterparts are not available. Optical depth retrievals for estimating the total water paths from satellites may be available in future IOPs. The comparison among the water species indicates that graupel is the most dominant species in mid-latitudes, while the other species contribute to the total

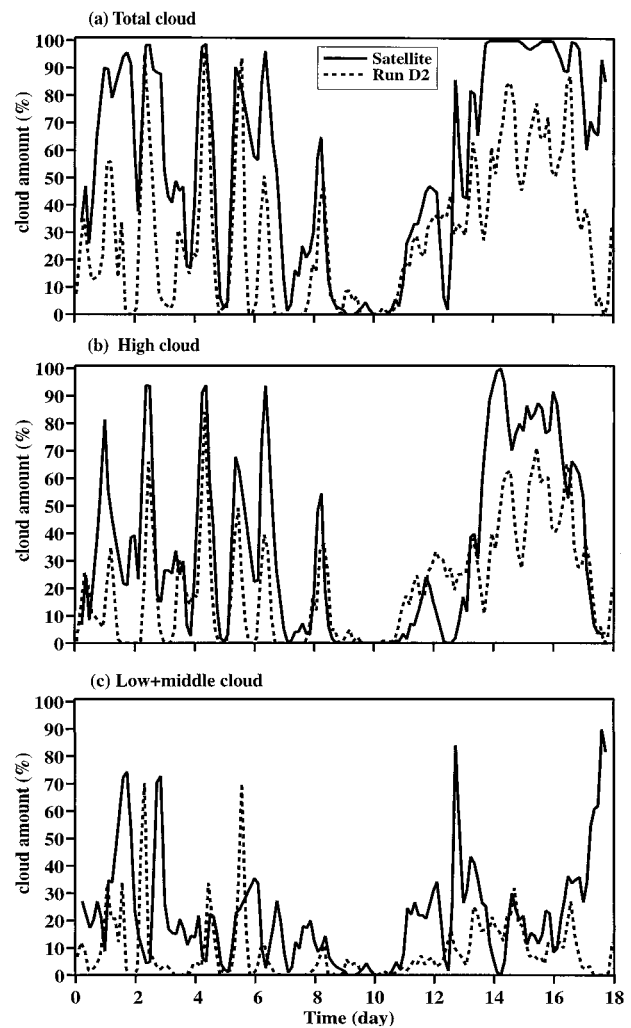


FIG. 11. Time sequence of domain-averaged (a) total cloud amount, (b) high ($>6 \text{ km}$) cloud amount, and (c) low + middle cloud amount from satellite observations and simulation D2.

condensate water more or less equally. The large amount of graupel is associated with the dry middle troposphere of large-scale midlatitude environment. The amount of graupel is far smaller during the last convectively active subperiod due to a moister, Tropics-like environment.

The satellite- (*GOES-7*) observed cloud amounts (Minnis et al. 1995) have been compared with the simulation (Fig. 11). The simulated cloud amounts are calculated, based upon the cloud-top height with a criterion (0.02 kg m^{-2} ; Cahalan et al. 1995; Harshvardhan et al. 1994) on the liquid water + ice path. The satellite procedure used the threshold method on the brightness temperature, which may overestimate low cloud amounts when the clouds are scattered, as for shallow cumuli. The simulated high and total cloud amounts agree with satellite observations rather well, in terms of their temporal correlation. The low and middle cloud amounts compare with observations far less favorably. This could

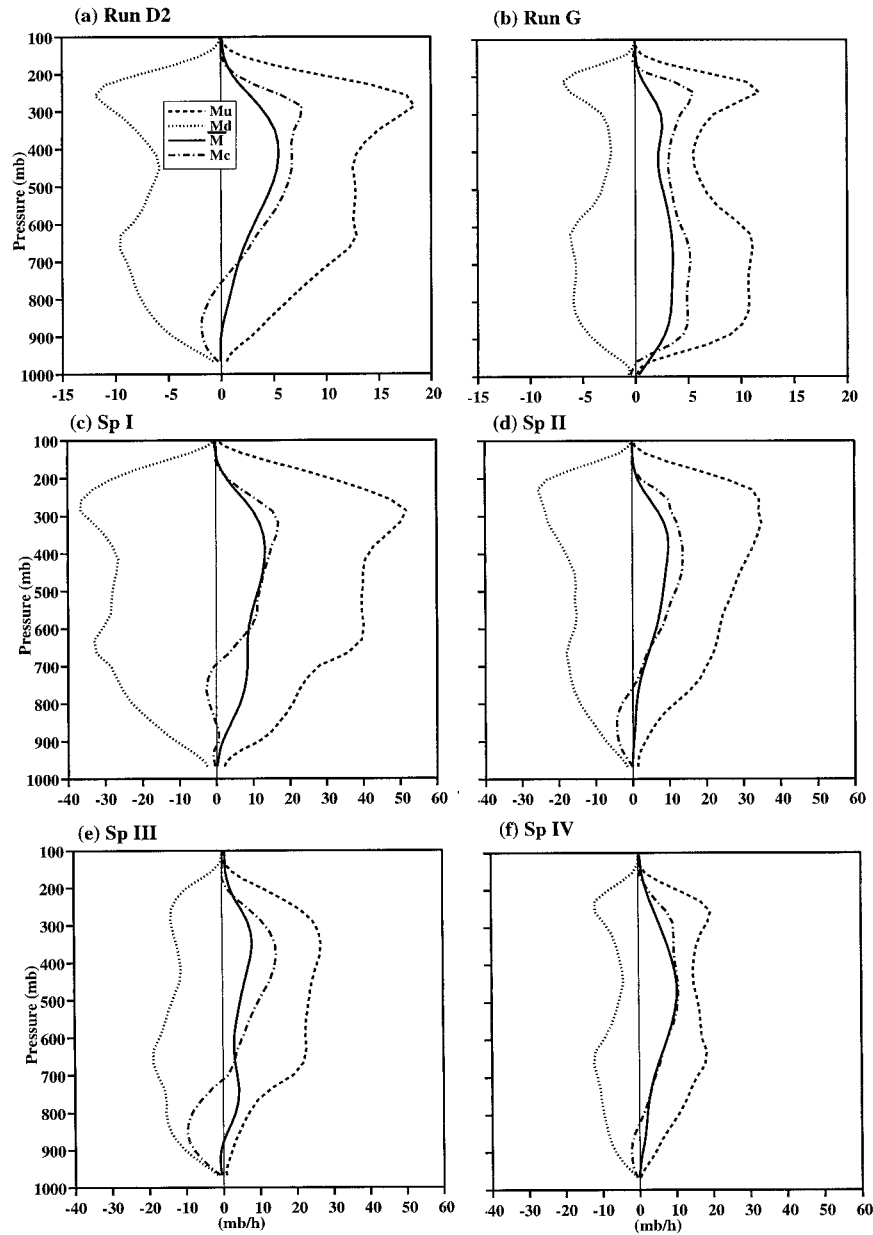


FIG. 12. Vertical profiles of the mean large-scale mass flux (\bar{M}), cumulus mass flux (M_c), updraft mass flux (M_u), and downdraft mass fluxes (M_d) for simulations (a) D2 and (b) G. (c), (d), (e), and (f) Selected subperiods from D2.

be related to the coarse horizontal resolution of the simulation and the lack of a turbulence-scale condensation scheme in the simulation (XR96). The comparison between CEM simulated and satellite observed cloud amounts is nevertheless encouraging although the underestimates of upper-level cloud amounts may also be related to the limited size of the model domain; that is, compensating downward motions of cloud systems are restricted within the model domain about 500 km wide.

Next, the mean updraft mass flux (M_u), downdraft mass flux (M_d), and the net cumulus mass flux (M_c) for

convectively active periods are compared with those of tropical cumulus convection (Fig. 12) because observational counterparts are not available. Inclusion of convectively inactive periods only changes the magnitudes of the mass fluxes, not their vertical shapes. The 18-day means of simulation G of GATE (XR96) are used to represent tropical convection because convection was active almost continuously during Phase III.

The net cumulus mass flux (M_c) in simulation D2 is downward in the lowest 200 mb and most strongly upward above 750 mb (Fig. 12a) in spite of the positive

large-scale mass fluxes (\overline{M}) throughout the troposphere. Such a structure is very different from that typically diagnosed in the Tropics (Yanai et al. 1973; Cheng 1989) or that simulated by the same CEM for the GATE Phase III (Fig. 12b). It was not diagnosed with the PRE-STORM dataset in spite of similar \overline{M} profiles (Wu 1993). This can be attributed to the weak downdraft activities and the assumption of a constant cloudbase height in the diagnostic study. The averaged planetary boundary layer (PBL) depths are, however, highly varying with time in midlatitudes (Fig. 10c). On the other hand, M_c and \overline{M} in the Tropics are much larger in the lower troposphere than in midlatitudes. Nevertheless, such an M_c profile in midlatitudes is consistent with that of the mean Q_1 profile shown in Fig. 9e.

The updraft mass flux (M_u) is large in the middle and upper troposphere but small in the lower troposphere. This is also very different from that of the GATE simulation, where the maximum M_u appears in the lower troposphere. Such a different structure suggests that the cloud spectra are significantly different although higher cloud bases in midlatitudes also contribute to the lower values of M_u (Fig. 10c). As first examined by Lewis (1975) and later confirmed by Wu (1993), the deep cumulus clouds are dominant in the cloud spectrum of midlatitude cumulus ensembles. On the other hand, M_d is relatively large in the lower troposphere, which is responsible for the negative M_c in the lowest 200 mb and associated evaporative cooling. The downdraft mass flux in the middle and upper troposphere is also much greater than that in the GATE simulation. However, some of the strong M_d and M_u around 250 mb are related to unrealistically, strong gravity wave activities in the simulation due to strong shear in the upper troposphere of midlatitudes. An analysis method for eliminating gravity wave contributions to M_d and M_u is highly desired, such as trajectory analysis (Krueger et al. 1995b; Lin and Arakawa 1997).

The mean mass flux profiles over the entire IOP do not shed much new light on the cloud spectrum of midlatitude cumulus convection. Thus, averaged profiles over four subperiods of the IOP are examined (Figs. 12c–f). Three 12-h periods on days 3, 7, and 9 and one 60-h period between days 14 and 17 are chosen (see Figs. 6 and 7), which are labeled as Sps (Subperiods) I, II, III, and IV in Fig. 12, respectively. As far as M_c is concerned, the differences among the subperiods are associated with the zero mass flux levels in the lower troposphere, due to the highly varying subcloud layer depths (Fig. 10c). Subperiod IV has the smallest negative M_c , which is related to the Tropics-like environment, with very low PBL depths (Fig. 12f), while Sp III has the largest negative M_c , with high PBL depths. The differences of M_u and M_d among the subperiods are related to 1) the different cloudbase heights and 2) the different cloud spectra. For example, both Sps II and III show very high cloudbase heights (Figs. 12d,e, 10c). Subperiod II also shows the most dominance of deep

cloud types because of the monotonic increase of M_u with height. During Sp IV, cumulus convection was heavily influenced by quasi-stationary tropical weather systems; namely, the remnants of Tropical Storm Dean. It is somewhat surprising that the characters of M_u and M_d for Sp IV are closer to those of mean tropical profiles (Fig. 12b) than those of Sps I, II, and III although the \overline{M} profile is not.

To further understand the differences between midlatitude and tropical convection, the vertical profiles of the heat and moisture budget components, that is, the convergences of the eddy heat and moisture transports and the phase change rates, are examined (Fig. 13). The mathematical expressions for these components can be found, for example, in Xu (1995). The mean convergences of the eddy heat transports (Figs. 13a,c) are small in both simulations D2 and G except for the lowest 150 mb. Recall that Q_1 is negative in the lowest 2 km in midlatitudes (Fig. 9b) but near zero in the Tropics. Thus, a larger net evaporative cooling as a result of stronger downdrafts and a drier atmosphere is the main cause for the negative Q_1 in midlatitudes (see Fig. 13c).

The mean convergences of the eddy moisture transports have some differences between midlatitudes and Tropics (Figs. 13b,d). The largest moistening rate due to eddy transports appears above the melting level (as indicated by the maximum phase change rate) in the Tropics but below the melting level (640 mb) in midlatitudes. A significant secondary maximum also appears at 400 mb in midlatitudes. These peaks determine the separation of the Q_1 and Q_2 maxima. There is also a much thicker layer of drying in the lowest 300 mb in midlatitudes than in the Tropics, which is responsible for the secondary maximum of Q_2 at approximately 900 mb (Fig. 9d). The thicker layer is related to the highly varying, deep subcloud layers in midlatitudes (Fig. 10c), which results in large transports of the drier downdraft air.

Individual subperiods show large variations in the vertical structures of the eddy heat convergences but substantially smaller variations of the eddy moisture convergences (not shown). In general, the convergences of the eddy heat transports in midlatitudes show more complicated vertical structures and much larger amplitudes of variations than the mean profile shown in Fig. 13c. On the other hand, the convergences of the eddy moisture transports are rather robust as in the 18-day mean profile; that is, drying in the lowest troposphere and moistening in the middle/upper troposphere, due to the exponential decrease of moisture with height in the atmosphere.

The individual phase change terms (Figs. 13e–g) show some differences in the upper troposphere between D2 and G. That is, the sublimation, deposition, melting, and freezing processes are rather similar between the Tropics and midlatitudes for the averaged profiles over the 18-day periods, which cannot be verified from observations. The most significant differences between the

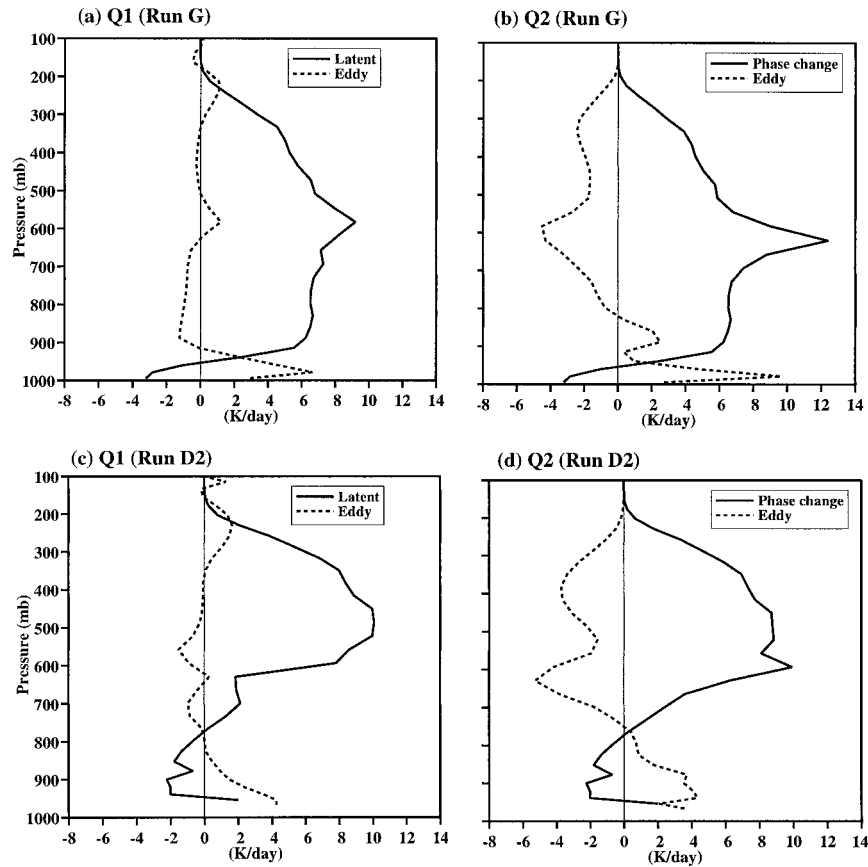


FIG. 13. (a), (b), (c), (d) Vertical profiles of the heat and moisture budget components for the entire period of simulations D2 and G.

two simulations appear in the condensation and evaporation rates. The condensation rate is much smaller in midlatitudes than in the Tropics, due to a smaller number of shallow clouds and possibly the higher cloud-base heights. The evaporation rates (sum of rainwater and cloudwater evaporation) are more comparable, in spite of the slightly drier midlatitude atmosphere, because evaporation of cloud water in D2 is rather small but very significant in G (not shown).

e. Radiative aspects

The 18-day mean OLR flux from simulation D2 is only 10 W m^{-2} higher than the observed (262 W m^{-2} vs 252 W m^{-2}). The simulated temporal variations in terms of standard deviations are about 10 W m^{-1} less than the observed (Fig. 14a). The temporal correlation coefficient between simulated and observed OLRs is 0.77. Comparison of Fig. 15a with Fig. 11b indicates that all overestimates (underestimates) of the OLR are related to the underestimates (overestimates) of high cloud amounts, not those of the total cloud amounts. The significant overestimates during convectively active

subperiods are related to the underestimates of high cloud amounts (Figs. 11b and 15a).

The simulated top-of-atmosphere (TOA) net downward solar radiative fluxes are reasonably close to the observed, except for some overestimates during the last convectively active period and some underestimates at local noon of other portions of the IOP (Figs. 14b and 15b). The simulated IOP mean (305 W m^{-2}) and standard deviations (355 W m^{-2}) are extremely close to the observed ($309 \pm 361 \text{ W m}^{-2}$). The high-frequency differences with magnitudes less than 100 W m^{-2} shown in Fig. 15b are likely to be caused by the temporal sampling differences between observations and simulations.

The surface downwelling solar radiative fluxes are, however, overestimated by the model during some convectively active portions of the IOP (Figs. 14c and 15c). The overestimates are very large, especially during early and late portions of the IOP. A possible explanation is based upon the underestimates of the total cloud amounts by the model (Fig. 11a). For example, the overestimates are rather small during convectively inactive portions or for those portions of the IOP with less un-

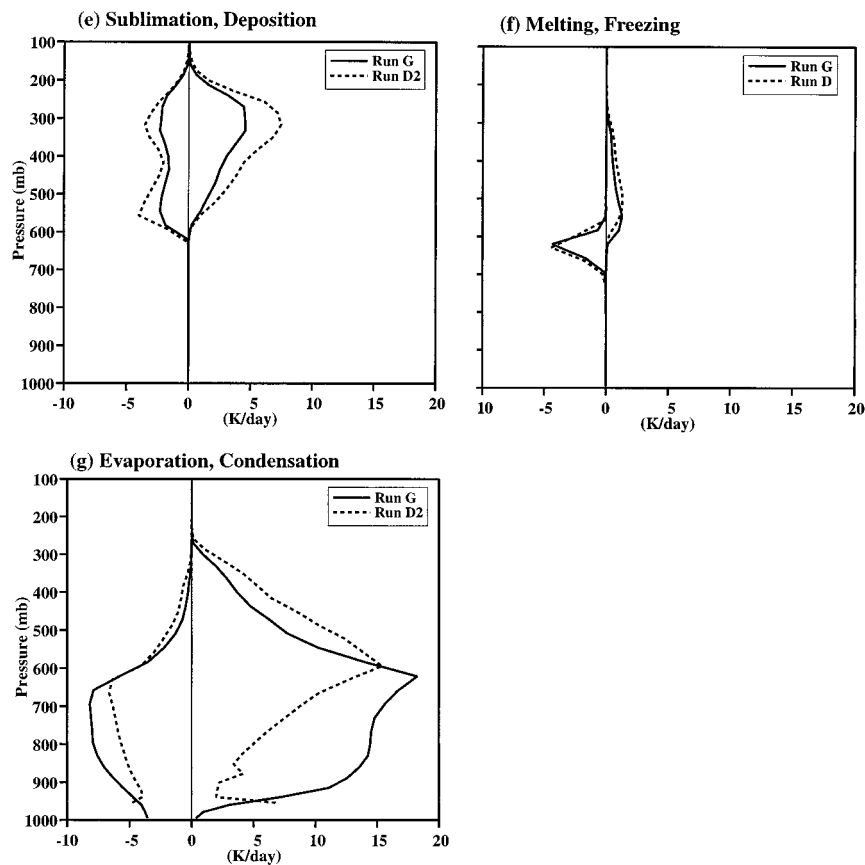


FIG. 13. (Continued) (e), (f), (g) The individual phase change terms.

derestimates of the total cloud amounts. Other possibilities are the lack of aerosol absorption in the radiation parameterization used in the UCLA-CSU CEM.

5. Summary and discussion

This study has presented some results from several simulations of cumulus ensembles at the Southern Great Plains site of the ARM program during the July 1995 IOP, as a part of the ARM single-column model inter-comparison study (Ghan et al. 2000). The UCLA-CSU cloud ensemble model (CEM) is used to explicitly simulate the macroscopic properties of midlatitude cumulus ensembles. A detailed comparison with available observations and tropical convection has been made in this study.

In general, the CEM-simulated results agree reasonably well with the available observations from the July 1995 IOP and better than those obtained from single-column models (Ghan et al. 2000). The simulated temperature and moisture differences from the observations are typically close to the observed variabilities of midlatitude atmosphere, especially during convectively active portions of the IOP. The simulated mean generalized convective available potential energy (GCAPE) during

convectively active periods is also comparable to the observed mean GCAPE. The simulated, domain-averaged precipitable water is within the uncertainties of data analysis. The simulated surface precipitation rate agrees with observations well. The temporal evolutions of the satellite-observed cloud amounts, OLR, and TOA solar fluxes compare well with those from the simulation.

The differences between simulated and observed temperature and moisture profiles, especially during convectively inactive portions of the IOP, are much larger than those obtained in tropical cases, for example, those based on the GATE Phase III data with the same CEM (XR96). As a result, the GCAPE of the simulated atmosphere is half of that observed during the same portions of the IOP.

In spite of the high temporal correlations between observed and simulated cloud amounts, the amplitudes of cloud amounts are severely underestimated, especially for the low-level clouds. The underestimate of low-level clouds can be partly attributed to the differences between satellite estimate and model diagnostics, as well as the lack of a subgrid-scale cloudiness parameterization in the simulation. These underestimates impact the simulated radiative fluxes at the TOA and the

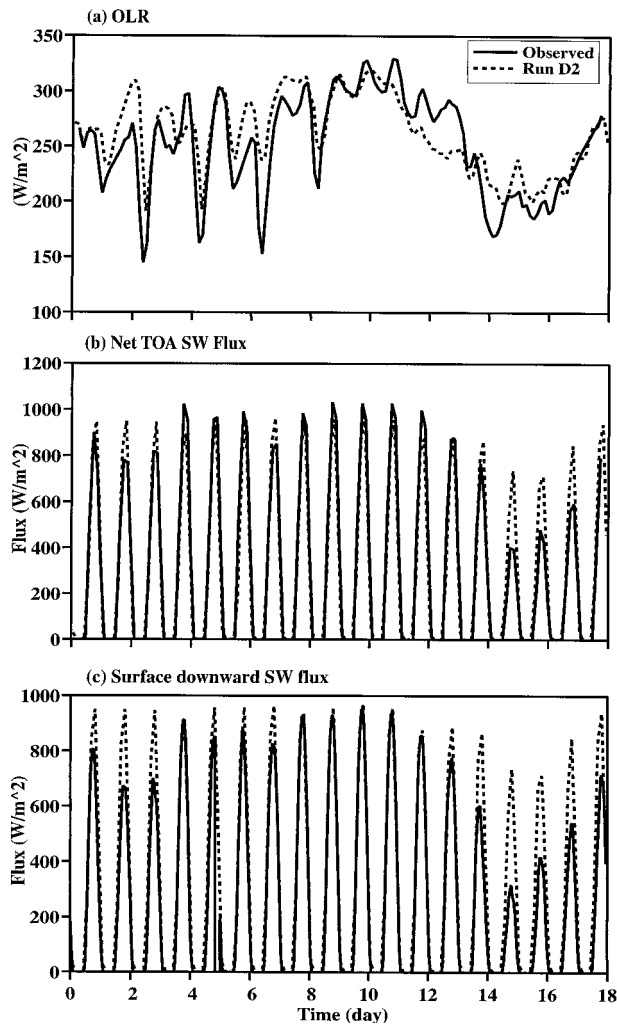


FIG. 14. Time sequences of selected variables in the radiative budgets: (a) OLR flux, (b) net TOA solar radiative flux, and (c) surface downwelling solar radiative flux from simulation D2 and observations.

surface, compared with satellite- and surface-based observations. The underestimates of upper-level cloud amounts may partly be related to the limited domain size of the model; that is, compensating downward motions of cloud systems are restricted within the model domain.

Significant differences between the statistical properties of tropical and midlatitude cumulus convection have been identified in this study, especially in the vertical profiles of the cumulus mass fluxes, apparent heat source (Q_1) and apparent moisture sink (Q_2), as well as the structures of MCSs. The strong variations of the subcloud-layer thermodynamic structure, the surface fluxes, the slightly drier environments and the frontal dynamics in midlatitudes have large impacts on the mass, heat, and moisture budgets. The cloud spectrum of cumulus ensembles in midlatitudes is more dominated by deep clouds, compared to tropical oceanic con-

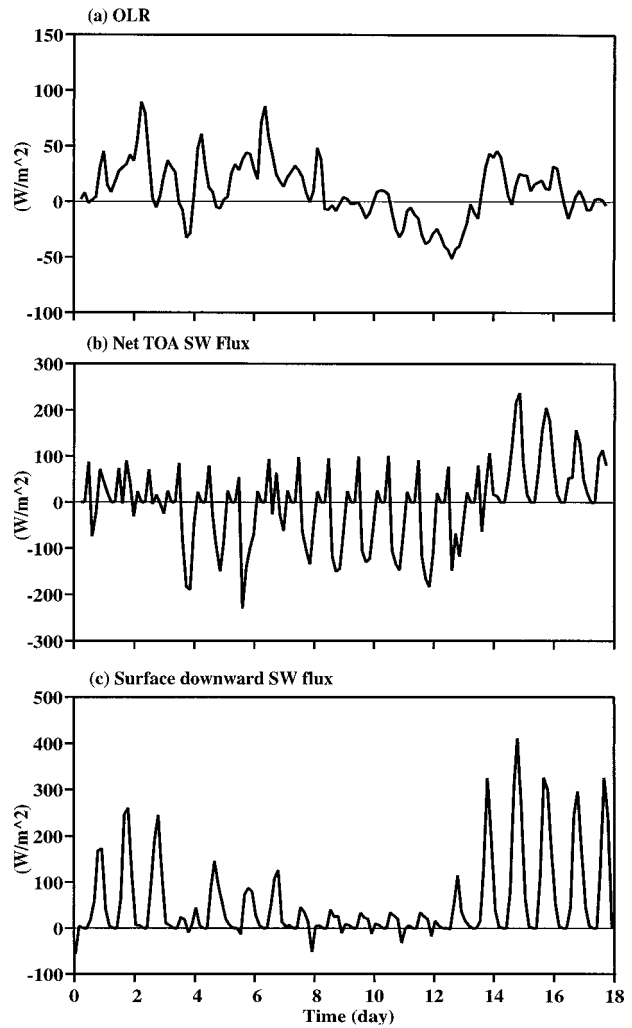


FIG. 15. Same as Fig. 14 except for the differences between model and observations.

vection. Because of the lack of shallow clouds and higher PBL depths, the net condensation rate is negative in the lowest 200 mb. The evaporative cooling is clearly linked to the downward cloud mass flux, which is usually positive in the maritime Tropics. Such a difference suggests that it is essential to have a downdraft component in a cumulus parameterization (e.g., Johnson 1976; Cheng and Arakawa 1997) to predict the cumulus feedbacks in midlatitudes correctly, as suggested also by the semiprognostic tests of Grell et al. (1991).

The results presented in this study represent the best among eight CEM simulations performed under the ARM SCM intercomparison study. Some deficiencies of the model and inadequate accuracy of large-scale advective tendencies can impact the simulated results, which are partially addressed in the sensitivity simulations. Apparent deficiencies such as the underestimate of low-level clouds are needed to be addressed in the future by performing additional sensitivity simulations.

Other deficiencies of the simulation are related to the limitations of the 2D model. For example, sensitivity tests in (XR96) reveal that 2D model has stronger inhibiting effects on convection and unrealistically efficient in vertical transports of heat, moisture, and momentum when the vertical shear of horizontal wind is strong. Nevertheless, this study has demonstrated that CEM-simulated results can be used to improve our understanding of midlatitude cumulus convection.

Acknowledgments. Observational datasets used in the present study were kindly provided by Professor Minghua Zhang of SUNY—Stony Brook, Dr. Ric Cederwall and Mr. John Yio of Lawrence Livermore National Laboratory, and Mr. Doug Cripe of Colorado State University. Discussions with Doug Cripe were very helpful. Comments by Professor Steven Krueger and an anonymous reviewer were very helpful for revising the manuscript.

This research was supported by the Environmental Sciences Division of the U.S. Department of Energy under Grant DE-FG03-95ER61968 as part of the Atmospheric Radiation Measurement Program. The computations were performed at the National Energy Research Supercomputer Center, Berkeley, California.

REFERENCES

- Arakawa, A., and W. H. Schubert, 1974: Interaction of a cumulus cloud ensemble with the large-scale environment. Part I. *J. Atmos. Sci.*, **31**, 674–701.
- Browning, K. A., 1994: *GEWEX Cloud System Study (GCSS) Science Plan*. IGPO Publication Series, Vol. 11, International GEWEX Project Office, 84 pp.
- Cahalan, R. F., D. Silberstein, and J. B. Snider, 1995: A validation of a satellite cloud retrieval during ASTEX. *J. Atmos. Sci.*, **52**, 3002–3012.
- Cheng, M.-D., 1989: Effects of downdrafts and mesoscale convective organization on the heat and moisture budgets of tropical cloud clusters. Part II: Effects of convective-scale downdrafts. *J. Atmos. Sci.*, **46**, 1540–1564.
- , and A. Arakawa, 1997: Inclusion of rainwater budget and convective downdrafts in the Arakawa–Schubert cumulus parameterization. *J. Atmos. Sci.*, **54**, 1359–1378.
- Cunning, J. B., 1986: The Oklahoma–Kansas Preliminary Regional Experiment for STORM-Central. *Bull. Amer. Meteor. Soc.*, **67**, 1478–1486.
- Doran, J. C., J. M. Hubbe, J. C. Liljegren, W. J. Shaw, G. J. Collatz, D. R. Cook, and R. L. Hart, 1998: A technique for determining the spatial and temporal distributions of surface fluxes of heat and moisture over the Southern Great Plains Cloud and Radiation Testbed. *J. Geophys. Res.*, **103**, 6109–6121.
- Gallus, W. A., Jr., and R. H. Johnson, 1991: Heat and moisture budgets of an intense midlatitude squall line. *J. Atmos. Sci.*, **48**, 122–146.
- Ghan, S., and Coauthors, 2000: An intercomparison of single column model simulations of summertime midlatitude continental convection. *J. Geophys. Res.*, **105**, 2091–2124.
- Grabowski, W. W., X. Wu, and M. W. Moncrieff, 1996: Cloud-resolving modeling of tropical cloud systems during Phase III of the GATE. Part I: Two-dimensional experiments. *J. Atmos. Sci.*, **53**, 3684–3709.
- Grell, G. A., Y.-H. Kuo, and R. J. Pasch, 1991: Semi-prognostic tests of cumulus parameterization schemes in the middle latitudes. *Mon. Wea. Rev.*, **119**, 5–31.
- Harshvardhan, R. Davies, D. A. Randall, and T. G. Corsetti, 1987: A fast radiation parameterization for general circulation models. *J. Geophys. Res.*, **92**, 1009–1016.
- , B. A. Wielicki, and K. M. Ginger, 1994: The interpretation of remotely sensed cloud properties from a model parameterization perspective. *J. Climate*, **7**, 1987–1998.
- Houze, R. A., and A. K. Betts, 1981: Convection in GATE. *Rev. Geophys. Space Phys.*, **19**, 541–576.
- , and P. V. Hobbs, 1982: Organization and structure of precipitating cloud systems. *Advances in Geophysics*, Vol. 24, Academic Press, 225–315.
- Johnson, R. H., 1976: The role of convective-scale precipitation downdrafts in cumulus and synoptic-scale interactions. *J. Atmos. Sci.*, **33**, 1890–1910.
- , 1993: Midlatitude convective systems. *Clouds and Climate, Notes from an NCAR Summer Colloquium*, Boulder, CO, NCAR, 245–286.
- Kreitzberg, C. W., and D. J. Perky, 1976: Release of potential instability. Part I: A sequential plume model within a hydrostatic primitive equation model. *J. Atmos. Sci.*, **33**, 456–475.
- Krueger, S. K., 1988: Numerical simulation of tropical cumulus clouds and their interaction with the subcloud layer. *J. Atmos. Sci.*, **45**, 2221–2250.
- , 1997: A GCSS intercomparison of cloud-resolving models based on TOGA COARE observations. *Proc. ECMWF/GCSS Workshop on New Insights and Approaches to Convective Parameterization*, Reading, United Kingdom, ECMWF, 113–127.
- , Q. Fu, K. N. Liou, and H.-N. Chin, 1995a: Improvements of an ice-phase microphysics parameterization for use in numerical simulations of tropical convection. *J. Appl. Meteor.*, **34**, 281–287.
- , G. T. McLean, and Q. Fu, 1995b: Numerical simulation of the stratus-to-cumulus transition in the subtropical marine boundary layer. Part II: Boundary-layer circulation. *J. Atmos. Sci.*, **52**, 2851–2868.
- Kuo, H. L., 1974: Further studies of the parameterization of the influence of cumulus convection on large-scale flow. *J. Atmos. Sci.*, **31**, 1232–1240.
- Kuo, Y.-H., and R. A. Anthes, 1984: Mesoscale budgets of heat and moisture in a convective system over the central United States. *Mon. Wea. Rev.*, **112**, 1482–1497.
- Leach, M. J., J. Yio, and R. T. Cederwall, 1996: Estimation of errors in objectively analyzed fields and sensitivity to number and spacing of stations. *Proc. Sixth Annual Atmospheric Radiation Measurement (ARM) Science Team Meeting*, San Antonio, TX, U.S. Department of Energy, 149–151.
- Lewis, J. M., 1975: Test of Ogura-Cho model on a prefrontal squall line case. *Mon. Wea. Rev.*, **103**, 764–778.
- Li, X., C.-H. Sui, K.-M. Lau, and M.-D. Chou, 1999: Large-scale forcing and cloud–radiation interaction in the tropical deep convective regime. *J. Atmos. Sci.*, **56**, 3028–3042.
- Liljegren, J. C., 1994: Two-channel microwave radiometer for observations of total column precipitable water vapor and cloud liquid water path. Preprints, *Fifth Symp. on Global Change*, Nashville, TN, Amer. Meteor. Soc., 262–269.
- Lin, C.-C., and A. Arakawa, 1997: The macroscopic entrainment processes of simulated cumulus ensemble. Part I: Entrainment source. *J. Atmos. Sci.*, **54**, 1027–1043.
- Lin, X., and R. H. Johnson, 1994: Heat and moisture budgets and circulation characteristics of a frontal squall line. *J. Atmos. Sci.*, **51**, 1661–1681.
- Lin, Y.-L., R. D. Farley, and H. D. Orville, 1983: Bulk parameterization of the snow field in a cloud model. *J. Climate Appl. Meteor.*, **22**, 1065–1092.
- Lord, S. J., H. E. Willoughby, and J. M. Piotrowicz, 1984: Role of a parameterized ice-phase microphysics in an axisymmetric, non-hydrologic tropical cyclone model. *J. Atmos. Sci.*, **41**, 2836–2848.

- Minnis, P., W. L. Smith Jr., D. P. Garber, J. K. Ayers, and D. R. Doelling, 1995: Cloud properties derived from *GOES-7* for spring 1994 ARM Intensive Observing Period using Version 1.0.0 of ARM satellite data analysis program. NASA Reference Publication 1366, 59 pp. [Available from NASA Langley Research Center, Hampton, VA 23681-0001.]
- Ogura, Y., and H.-R. Cho, 1973: Diagnostic determination of cumulus populations from large-scale variables. *J. Atmos. Sci.*, **30**, 1276–1286.
- , and J.-Y. Jiann, 1985: A modeling study of heating and drying effects of convective clouds in an extratropical mesoscale convective system. *J. Atmos. Sci.*, **42**, 2478–2492.
- Ooyama, K., 1987: Scale-controlled objective analysis. *Mon. Wea. Rev.*, **115**, 2476–2506.
- Randall, D. A., and D. G. Cripe, 1999: Alternative methods for specification of observed forcing in single-column models and cloud system models. *J. Geophys. Res.*, **104**, 24 527–24 545.
- , K.-M. Xu, R. C. J. Somerville, and S. Iacobellis, 1996: Single-column models and cloud ensemble models as links between observations and climate models. *J. Climate*, **9**, 1683–1697.
- Redelsperger, J.-L., and Coauthors, 2000: A GCMSS model intercomparison for a tropical squall line observed during TOGA-COARE. I. Cloud-resolving models. *Quart. J. Roy. Meteor. Soc.*, **126**, 823–863.
- Schlesinger, R. E., 1994: Heat, moisture and momentum budgets of isolated deep midlatitude and tropical convective clouds as diagnosed from three-dimensional model output. Part I: Control experiment. *J. Atmos. Sci.*, **51**, 3649–3673.
- Sellers, P. J., and Coauthors, 1996: A revised land-surface parameterization (Sib2) for atmospheric GCMs. Part I: Model formulation. *J. Climate*, **9**, 676–705.
- Soong, S.-T., and W.-K. Tao, 1980: Response of deep tropical cumulus clouds to mesoscale processes. *J. Atmos. Sci.*, **37**, 2016–2034.
- Stephens, G. L., S.-C. Tsay, P. W. Stackhouse Jr., and P. J. Flatau, 1990: The relevance of the microphysical and radiative properties of cirrus clouds to climate and climate feedback. *J. Atmos. Sci.*, **47**, 1742–1753.
- Stokes, G. M., and S. E. Schwartz, 1994: The Atmospheric Radiation Measurement (ARM) program: Programmatic background and design of the cloud and radiation test bed. *Bull. Amer. Meteor. Soc.*, **75**, 1202–1221.
- Tao, W.-K., J. Simpson, C.-H. Sui, B. Ferrier, S. Lang, J. Scala, M.-D. Chou, and K. Pickering, 1993: Heating, moisture and water budgets of tropical and midlatitude squall lines: Comparisons and sensitivity to longwave radiation. *J. Atmos. Sci.*, **50**, 673–690.
- , S. Lang, J. Simpson, M.-D. Chou, Y. Wang, C.-H. Sui, and B. Ferrier, 1996: Mechanisms of cloud–radiation interaction in the Tropics and midlatitudes. *J. Atmos. Sci.*, **53**, 2624–2651.
- Thompson, R. M., Jr., S. W. Payne, E. E. Recker, and R. J. Reed, 1979: Structure and properties of synoptic-scale wave disturbances in the intertropical convergence zone of the eastern Atlantic. *J. Atmos. Sci.*, **36**, 53–72.
- Wang, J., and D. A. Randall, 1994: The moist available energy of a conditionally unstable atmosphere. Part II: Further analysis of GATE data. *J. Atmos. Sci.*, **51**, 703–710.
- Wu, X., 1993: Effects of cumulus ensemble and mesoscale stratiform clouds in midlatitude convective systems. *J. Atmos. Sci.*, **50**, 2496–2518.
- Wu, X., W. W. Grabowski, and M. W. Moncrief, 1998: Long-term behavior of cloud systems in TOGA COARE and their interactions with radiative and surface processes. Part I: Two-dimensional modeling study. *J. Atmos. Sci.*, **55**, 2693–2714.
- Xu, K.-M., 1995: Partitioning mass, heat and moisture budgets of explicitly simulated cumulus ensembles into convective and stratiform components. *J. Atmos. Sci.*, **52**, 551–573.
- , and S. K. Krueger, 1991: Evaluation of cloudiness parameterizations using a cumulus ensemble model. *Mon. Wea. Rev.*, **119**, 342–367.
- , and D. A. Randall, 1995: Impact of interactive radiative transfer on the macroscopic behavior of cumulus ensembles. Part I: Radiation parameterization and sensitivity test. *J. Atmos. Sci.*, **52**, 785–799.
- , and —, 1996: Explicit simulation of cumulus ensembles with the GATE Phase III data: Comparison with observations. *J. Atmos. Sci.*, **53**, 3710–3736.
- , A. Arakawa, and S. K. Krueger, 1992: The macroscopic behavior of cumulus ensembles simulated by a cumulus ensemble model. *J. Atmos. Sci.*, **49**, 2402–2420.
- Yanai, M., S. Esbensen, and J.-H. Chu, 1973: Determination of bulk properties of tropical cloud clusters from large-scale heat and moisture budgets. *J. Atmos. Sci.*, **30**, 611–627.
- Zhang, M. H., 1998: Integrating ARM measurements to force and evaluate GCM parameterizations. *Proc. Eighth Atmospheric Radiation Measurement (ARM) Science Team Meeting*, Tucson, AZ, U.S. Dept. of Energy, 847–851.
- , and J. L. Lin, 1997: Constrained variational analysis of sounding data based on column-integrated budgets of mass, heat, moisture, and momentum: Approach and application to ARM measurements. *J. Atmos. Sci.*, **54**, 1503–1524.